Journal of Materials Chemistry C

Accepted Manuscript

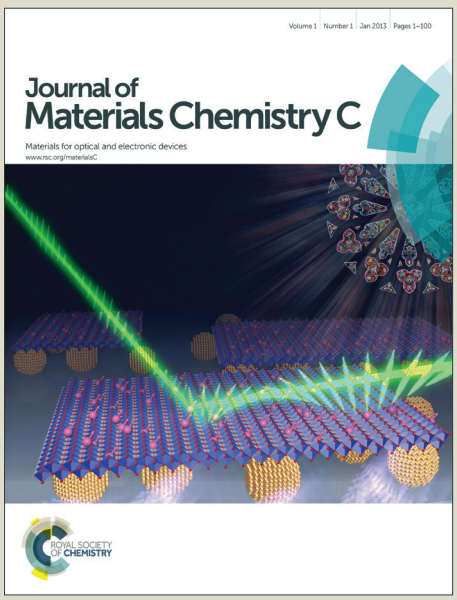

ROYAL SOCIETY OF CHEMISTRY

www.rsc.org/materialsC

Journal Name

RSCPublishing

ARTICLE

High colour rendering index and colour stable hybrid white efficient OLEDs with a double emitting layer structure using single phosphorescence dopant of heteroleptic platinum complexes

Cite this: DOI: 10.1039/x0xx00000x

Received ooth January 2012,
Accepted ooth January 2012

DOI: 10.1039/x0xx00000x

www.rsc.org/

Anurach Poloek,[abc] Chiao-Wen Lin,[a] Chin-Ti Chen,*[a] and Chao-Tsen Chen*[c]

Four heteroleptic platinum complexes (**FPtXND**) bearing 4-hydroxy-1,5-naphthyridine derivatives functionalized with dimethyl (**X** = **mm**), phenoxy (**X** = **OPh**), piperidine (**X** = **pp**), or carbazole (**X** = **Cz**) unit as one ligand (**XND**) and 2-(2,4-difluorophenyl)pyridine as the other common ligand (**F**) were newly synthesized and characterized. The crystal structures of **FPtOPhND** and **FPtCzND** were determined by the single-crystal X-ray diffraction crystallography. Although having short plane-to-plane packing distance of 3.62 and 3.39 Å, respectively, both platinum complexes have different molecular packing pattern, which affects the photoluminescence (PL) in solution and electroluminescence (EL) in solid state. Due to the contribution from both monomers and excimer/aggregate, all platinum complexes exhibited broad and red-shifted PL in concentrated solution as well as in doped thin film. In the monochromatic organic lighting diode (OLED) testing, **FPtXND** doped in 4,4'-di(9*H*-carbazol-9-yl)-1,1'-biphenyl (CBP) exhibited greenish yellow or orange yellow EL, of which **FPtOPhND** has the highest EL efficiency mainly due to its high solution PL quantum yield of 21%. Hybrid white OLEDs were first achieved with single emitting layer configuration, of which highly fluorescent blue *N*,*N*′-di-1-naphthalenyl-*N*,*N*′-diphenyl-[1,1′:4′,1″:4″,1‴-quaterphenyl]-4,4‴-diamine (4P-NPD) was used as the host material for all four platinum complexes. To improve the performance of the **FPtOPhND**-based hybrid white OLEDs, double emitting layer configuration were adopted with CBP and 4P-NPD as the host material, respectively. Virtually voltage independent, a white EL having $CIE_{x,y}$ (0.33, 0.31) and a CRI as high as 91 were obtained. Maximum EL efficiency of 11.8%, 25.9 cd A^{-1}, or 11.6 lm W^{-1} has been acquired with **FPtOPhND** doped in double emitting layer configuration of OLED.

Introduction

In the past few decades, white organic light-emitting diodes (WOLEDs) have drawn increasing attention because of their potential applications in full colour flat-panel displays and solid-state lighting.[1] In order to achieve white light emission, two or three emitters are generally required in device configuration. Particularly, three phosphorescent dopants (red, green, blue) have been employed to realise high electroluminescence (EL) efficiency and high quality (high colour rendering index, CRI) WOLEDs.[2] Nonetheless, the success of such WOLEDs hinges on complicated device structure which is difficult to be fabricated. Moreover, blue phosphorescent dopants still suffer from poor stability and frustration of finding suitable host materials due to their intrinsically high triplet energy (E_T) over 2.7 eV of iridium(III) bis[(4,6-difluorophenyl)-pyridinato-N,C^2]picolinate (FIrpic).[3] To simplify WOLED fabrication, utilizing only two complementary phosphorescent emitters, either blue and yellow or blue and orange,[4,5] is a reasonable alternative to achieve white electroluminescence (EL). In order to achieve stable WOLEDs and yet having easy fabrication, fluorescence (F)-phosphorescence (P) hybrid WOLEDs have been demonstrated before.[6] More recently, Leo et al. have reported a breakthrough of F-P hybrid WOLED by harnessing the separation of singlet and triplet excitons.[7] High performance *N*,*N*′-di-1-naphthalenyl-*N*,*N*′-diphenyl-[1,1′:4′,1″:4″,1‴-quaterphenyl]-4,4‴-diamine (4P-NPD) was used as the blue fluorescent material and the host for orange phosphorescent dopant $Ir(MDQ)_2(acac)$. 4P-NPD has a high photoluminescence (PL) quantum yield (92%) and sufficient triplet energy (E_T) of 2.3 eV for orange phosphorescent dopant. Since then, there have been numerous reports for such F-P hybrid WOLEDs and most of them

[a] *Institute of Chemistry, Academia Sinica, Taipei, Taiwan 11529, Republic of China. E-mail: chintchen@gate.sinica.edu.tw; Fax: +886 2 27831237; Tel: +886 2 27898542*
[b] *Nano Science and Technology Program, Taiwan International Graduate Program (TIGP), Academia Sinica and National Taiwan University*
[c] *Department of Chemistry, National Taiwan University, Taipei, Taiwan 10617*

† Electronic Supplementary Information (ESI) available: Synthesis, characterization and device performances. See DOI: 10.1039/b000000x/

are based on iridium complexes.[8] Although F-P hybrid WOLEDs with iridium complexes exhibit relatively high EL efficiency, insufficient CRI less than 80 is always the results. To improve the quality (i.e., CRI) of F-P hybrid WOLED with a simple device configuration, platinum complex is a better choice than iridium complex.[9] This is because platinum complexes, molecules having square planar geometry, are prone to aggregation in solid state, which often displays broadened EL spectrum due to its monomeric and excimeric emission.[10] Thus, WOLEDs with high CRI can be easily obtained when combined with a blue fluorescent host material. Accordingly, we have reported that high performance F-P hybrid WOLEDs can be achieved with a new heteroleptic platinum complex **FPtmND** (Scheme 1) and the blue fluorescent host 4P-NPD.[11] From such simple structure F-P WOLEDs, external quantum efficiency (EQE) or power efficiency (PE) as high as 11.9% or 12.1 lm W^{-1}has been obtained and a CRI as high as 89 was acquired as well. However, such a F-P hybrid device showed a warm white EL with $CIE_{x,y}$ (0.41, 0.41) and its colour stability needs to be demonstrated. Therefore, there is still room for improvement on such hybrid white OLEDs.

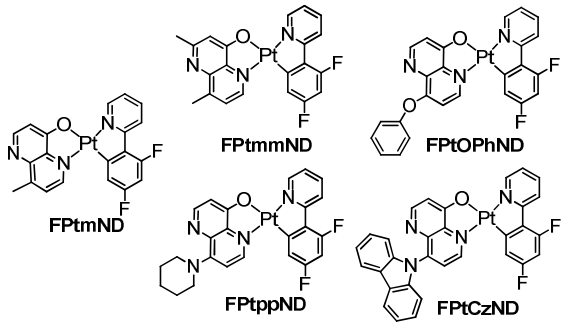

Scheme 1 Chemical structures of parent FPtmND and the functionalized platinum complexes (**FPtXND**).

In this contribution, we report the synthesis and characterization as well as photophysical, and electrochemical properties of a new class of heteroleptic platinum complexes **FPtXND,** where **X** = **mmND**, **OPhND**, **ppND** and **CzND** (Scheme 1). In the present study, hydroxyl-1,5-napthyridine ligands were functionalized with dimethyl, phenoxy, piperidino, or carbazolyl unit with the aim of tuning emission energy in solution and in solid state. Interestingly, all these platinum complexes display varied emission from greenish yellow to red wavelength due to its monomer and aggregate/excimer emission. We have found that the colour of which could be varied by controlling the concentration of dopant and the type of host materials in solid thin film. Different electroluminescent profiles were achieved with platinum complexes doped in either conventional host 4,4'-di(9*H*-carbazol-9-yl)-1,1'-biphenyl (CBP) or the new host (for platinum complexes) 4P-NPD. Hybrid white OLEDs were developed with a simple device configuration by utilizing monomer and excimer/aggregate emission of platinum complexes together with blue fluorescence of 4P-NPD.

Results and discussion

Synthesis

Pyridiylamine derivatives $\mathbf{4_{OPh}}$, $\mathbf{4_{pp}}$, and $\mathbf{4_{Cz}}$ are required in the preparation of heteroleptic platinum coordinated ligand **mmND**, **OPhND**, **ppND**, or **CzND**. They were readily prepared by adopting the literature procedure (Scheme 2) and ESI contains the synthetic detail and structural characterization data. In synthesizing hydroxyl-1,5-napthyridine derivatives, a facile two-step synthesis, namely Cassis method using Meldrum's acid in the first step and followed by heat-assisted intramolecular cyclization, has been developed before by us (Scheme 3).[12] Similar to many others, the new heteroleptic platinum complexes were prepared in two steps as shown in Scheme 3. It involved the cyclometallation of K_2PtCl_4 with 2-(2,4-difluorophenyl)pyridine (**F**) to form the Pt μ-dichloro-bridged dimer $\mathbf{(FPtCl)_2}$.[13] The subsequent reaction of $\mathbf{(FPtCl)_2}$ with **mmND**, **OPhND**, **ppND**, and **CzND** yielded heteroleptic platinum complexes **FPtmmND**, **FPtOPhND**, **FPtppND**, and **FPtCzND**, respectively. Details of synthetic of platinum complexes are given in experimental section.

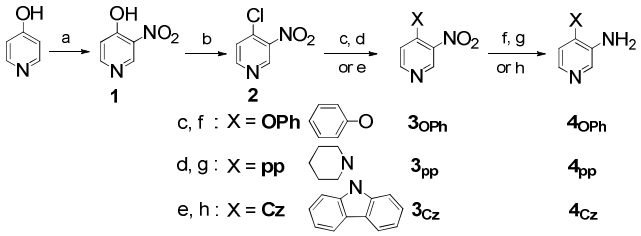

Scheme 2 Synthesis of pyridiylamine derivatives $\mathbf{4_{OPh}}$, $\mathbf{4_{pp}}$, and $\mathbf{4_{Cz}}$. Reagents, conditions and yields: (a) H_2SO_4, KNO_3, 100 °C, 92%; (b) $POCl_3$, toluene, 110 °C, 90%; (c) phenol, K_2CO_3, DMF, 80 °C, 95%; (d) piperidine, EtOH, 94%; (e) carbazol, Cs_2CO_3, MeCN, 82 °C, 62%; (f) $SnCl_2{\cdot}2H_2O$, HCl, MeOH, 80 °C, 85%; (g) cat. 10% Pd/C, H_2, THF, rt, 85%; (h) N_2H_4, cat. 10% Pd/C, EtOH/THF = 1:1, 92%.

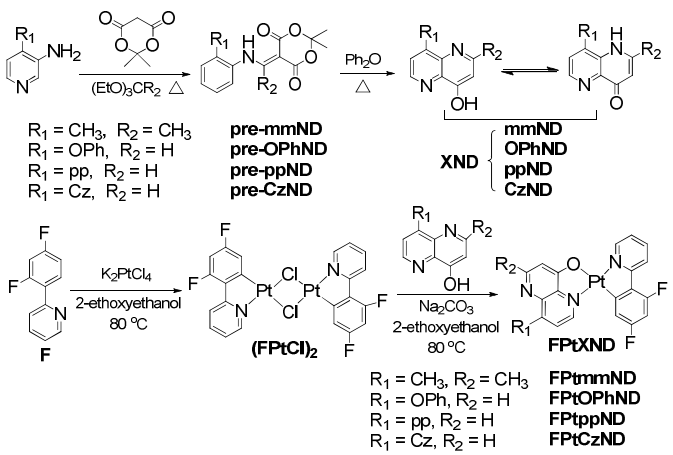

Scheme 3 Synthetic route of a series of 8-hydroxy-1,5-naphthyridine ligands **XND** and the corresponding platinum complexes **FPtXND**.

X-ray crystallography

Single crystals of **FPtOPhND** and **FPtCzND** were grown from dichloromethane/methanol solution. The molecular structure and molecular packing structure were acquired by single-crystal X-ray diffraction analysis.[14] Fig. 1 and 2 display the ORTEP diagram and stacking diagram of **FPtOPhND** and **FPtCzND**, respectively. The molecular structure of both **FPtOPhND** and **FPtCzND** exhibits a distorted square planar geometry with the two coordinating nitrogen atoms in *trans* conformation. The corresponding Pt-N, Pt-C and Pt-O distances are not so different for both complexes (see figure caption of both Fig. 1 and 2). However, the stacking diagrams show very different molecular packing of **FPtOPhND** and **FPtCzND**. For **FPtOPhND,** each molecule stacks almost on top of each other (Fig. 1 bottom left and right), having ~66.81° horizontal rotation along the stacking axis to avoid the eclipse configuration among adjacent molecules. A single uniformed Pt-Pt distance of 3.54 Å is found for the molecular stacking of **FPtOPhND**. An average plane-to-plane

distance of 3.62 Å is calculated for **FPtOPhND**. Such Pt-Pt distance is within a range of 3.15 to 3.76 Å reported by other dimeric structure of platinum complexes.[15] Very differently, **FPtCzND** molecules are stacked pair wise and each stacking pair is slided side way to form a slope packing from one direction (Fig. 2 bottom left). Similar to that of **FPtOPhND**, a ~44.85° horizontal rotation to avoid the eclipse configuration in each stacked pair. For each stacked pair of **FPtCzND**, the Pt-Pt distance is 3.17 Å (5.42 Å of the adjacent pairs) and an average plane-to-plane distance is 3.39 Å. In fact, both distances are shorter for **FPtCzND** than **FPtOPhND**. From single crystal x-ray analysis, the tighter and pair wise molecular packing observed for **FPtCzND** probably manifest its EL spectra, which are relatively narrow and the variation of EL wavelength is less dopant concentration dependent (see the section of EL properties).

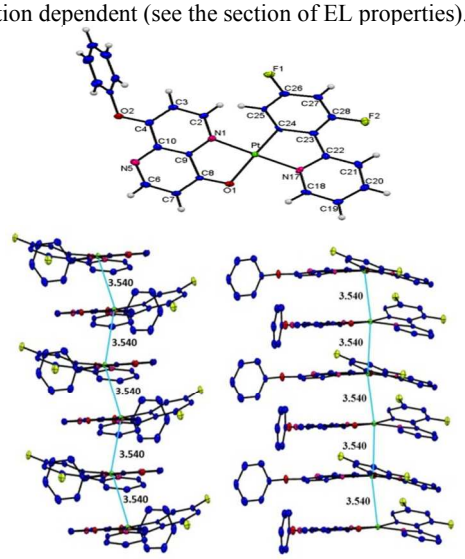

Fig. 1 ORTEP diagram of **FPtOPhND** with thermal ellipsoids shown at the 50% probability level (top). Stacking diagram (from two viewing angles ~90° difference) with an emphasis on the almost linear and exactly same Pt-Pt distance depicted with sky blue lines (bottom). Selected bond lengths (Å): Pt-N(1) = 2.022, Pt-O(1) = 2.120, Pt-N(17) = 1.990, Pt-C(24) = 1.978. In the stacking diagram, all hydrogen atoms are removed for clarity.

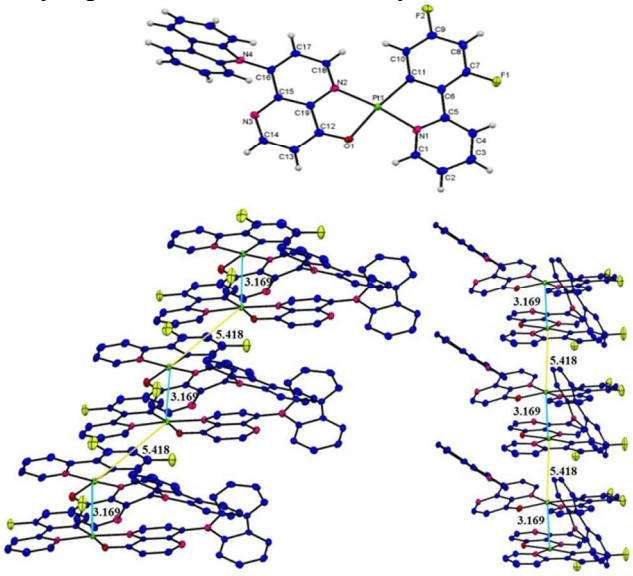

Fig. 2 ORTEP diagram of **FPtCzND** with thermal ellipsoids shown at the 50% probability level (top). Stacking diagram (from two viewing angles ~90° difference) with an emphasis on the two Pt-Pt distances, 3.17Å (sky blue lines) and 5.42 Å (golden yellow lines) (bottom). Selected bond lengths (Å): Pt-N(2) = 2.048, Pt-O(1) = 2.081, Pt-N(1) = 1.998, Pt-C(11) = 2.000. In the stacking diagram, all hydrogen atoms are removed for clarity.

UV-Visible absorption spectroscopic analysis

The UV-Visible absorption spectra of platinum complexes in CH_2Cl_2 at 1×10^{-5} M are shown in Fig. 3. These platinum complexes exhibit two types of absorption bands. The strong absorption band below 300 nm is attributed to the π-π^* local transition (LC) of the ligands. Except for **FPtppND**, each platinum complex shows multiple and weaker absorption bands in a range of 300-475 nm, which are assigned to some mixed electronic transitions of singlet metal-to-ligand charge transfer (^{1}MLCT) and triplet metal-to-ligand charge transfer (^{3}MLCT). Differently, the lowest energy (the longest wavelength) one among the multiple absorption bands in the range of 300-475 nm becomes much stronger in absorbance (Fig.3). This strong absorption band can be ascribed to mixed electronic transitions of ^{1}MLCT and intraligand charge transfer (ILCT), which is induced by the strong electron-donating piperidino amine substituent.[16]

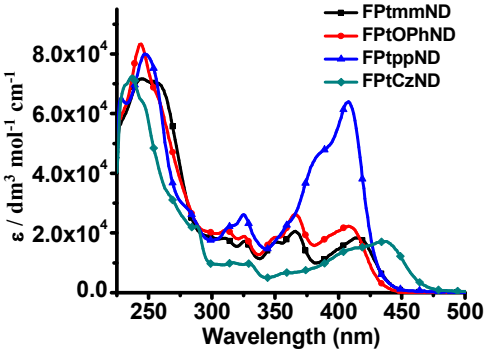

Fig. 3 UV-Vis absorption spectra of **FPtXND** in CH_2Cl_2 at a concentration of 1×10^{-5} M.

On the other hand, the absorption spectra of these platinum complexes can be either red-shifted or blue-shifted relative to those of the previously reported **FPtmND** or new **FPtmmND** reported herein, depending on the electron donating nature of the substituent. The strong electron donating ability of piperidino substituent shows the largest blue-shifting on the absorption band with the longest wavelength, whereas less stronger electron donating phenoxy substituent exhibits the second largest blue-shifting. Different from **FPtOPhND** and **FPtppND**, **FPtCzND** shows substantial red-shifted instead of blue-shifted absorption spectrum, even though carbazolyl moiety is an electron donating group. The twisted conformation of **CzND** largely inhibit tangible π-conjugation between 1,5-naphthyridine and carbazole moiety, and carbazole substituent of **FPtCzND** becomes an electron acceptor due to the relatively higher electron negativity of nitrogen atom. Single crystal x-ray structure of **FPtCzND** (Fig. 2) confirm the model of twisted conformation of **CzND**.

Photoluminescence spectroscopic analysis

The emission spectra of platinum complexes in solution with varied concentration are shown in Fig. 4 and Table 1. In a dilute solution of CH_2Cl_2 at 2×10^{-5} M, **FPtmmND**, **FPtOPhND** and **FPtppND** exhibit a greenish-yellow PL with λ_{max}^{PL} at 550, 555 and 545 nm,

Table 1 Photophysical data and thermal decomposition temperature of **FPtXND**.

Pt complexes	λ_{max}^{ab} (ε) [nm] in CH_2Cl_2 [10^4 M^{-1} cm^{-1}]	λ_{max}^{PL} [nm] in CH_2Cl_2			Φ_{PL} [a]	τ_p [b] [μs]	T_d [c] [°C]
		$2x10^{-5}$ M	$2x10^{-4}$ M	$2x10^{-3}$ M			
FPtmmND	415 (1.81)	550	572	593	0.09, 0.15	5.68	304
FPtOPhND	409 (2.25)	555	575	591	0.21, 0.10	6.12	319
FPtppND	407 (6.40)	545	545	578	0.08, 0.15	5.61	351
FPtCzND	437 (1.72)	573	573	579	0.15, 0.04	25.16	392

[a] PL quantum yields determined in degassed CH_2Cl_2 and 5 wt% in PS thin film.
[b] Room temperature PL lifetime determined in degassed CH_2Cl_2
[c] Thermal decomposition temperature (at 5% weight loss) determined by TGA under nitrogen atmosphere.

respectively, whereas **FPtCzND** displays an orange PL with λ_{max}^{PL} at 573 nm. At such diluted concentration, each of the platinum complexes can be presumed in non-aggregated form, i.e., monomer instead of dimer, trimer, and higher aggregates. Except for **FPtOPhND**, the emission wavelength shifting is in general parallel to that of absorption wavelength. When the concentration of platinum complex is increased, all emission spectra display a consistent trend of red-shifting and broadening (Fig. 4 and Table 1), which indicates the formation of aggregates showing variable excimer emission in solution. Within the context, the observation of excimer emission of **FPtCzND** takes place at higher concentration than the other three platinum complexes, which is consistent with the twisted (bulky) conformation of **CzND** that reduces the tendency of molecular aggregation in average. Such aggregation-inhibited conformation reduces the emission of aggregation, which usually has a wavelength greater than 625 nm or so (see solid state PL spectra in Fig. 6 later). Accordingly, under the same solution concentration, **FPtCzND** has a weaker PL intensity at long wavelength region around 625~700 nm because of less formation of aggregate/excimer in solution. As the results, **FPtCzND** exhibits the second weakest PL among **FPtXND** at wavelength beyond 625 nm (see Fig. 5 for the normalized solution PL spectra under the same concentration).

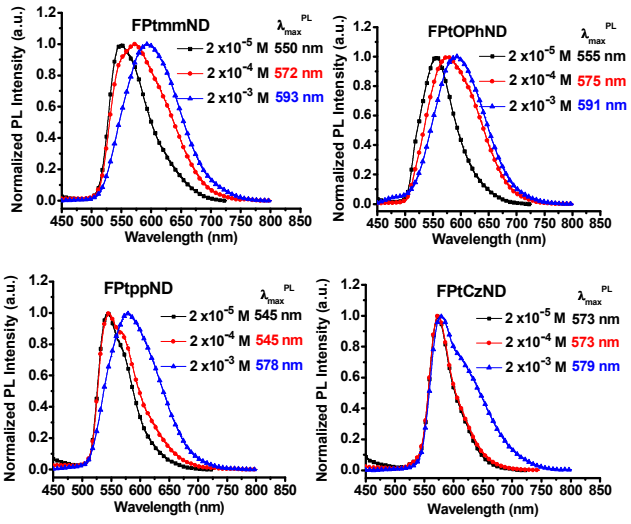

Fig. 4 Normalized emission spectra of **FPtmmND**, **FPtOPhND**, **FPtppND**, and **FPtCzND** in CH_2Cl_2 with varied concentrations.

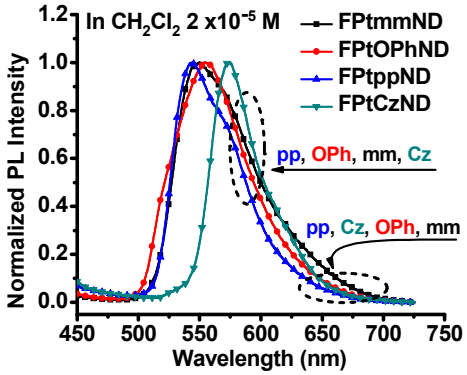

Fig. 5 Intensity normalized PL spectra of **FPtmmND**, **FPtOPhND**, **FPtppND**, and **FPtCzND** in CH_2Cl_2 at 2×10^{-5} M.

In the solid state, emission or PL spectra of platinum complexes display a variety of emission, depending on the concentration of platinum complex or type of host material incorporating platinum complex. Fig. 6 depicts the thin film PL spectra of **FPtXND** in polystyrene (PS), CBP, or 4P-NPD as the host materials. For 5 wt% of all **FPtXND** in CBP or PS hosted thin film, Fig. 6 show similar emission to the corresponding PL of **FPtXND** (λ_{max}^{PL} 530~575 nm) in diluted solution. However, in 4P-NPD hosted thin film, all platinum complexes exhibit more red-shifted PL spectra with λ_{max}^{PL} varied in a range of 575-650 nm. Moreover, even more red-shifted PL spectra are observed (some of them have λ_{max}^{PL} beyond 650 nm) in 100 wt% **FPtXND** for all platinum complexes. Regardless which host materials, the red-shifted emissions in thin film are attributed to the aggregation of **FPtXND**, similar to many other platinum complexes in the solid state. This observation is in good agreement with the molecular packing of **FPtOPhND** and **FPtCzND**, of which the average plane-to-plane distance is 3.62 and 3.39 Å, respectively. As a result, the close packing would facilitate the formation of dimer or higher aggregates. This gives rise of the emission around 579-640 nm because of metal-metal-to-ligand charge transfer transition (MMLCT) .[17]

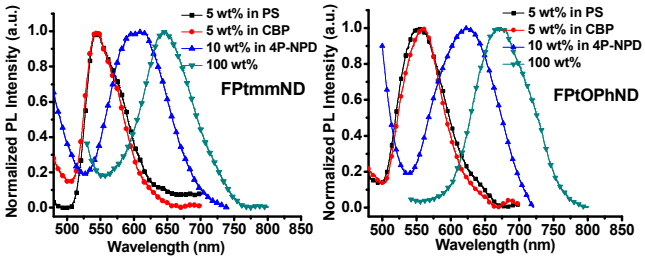

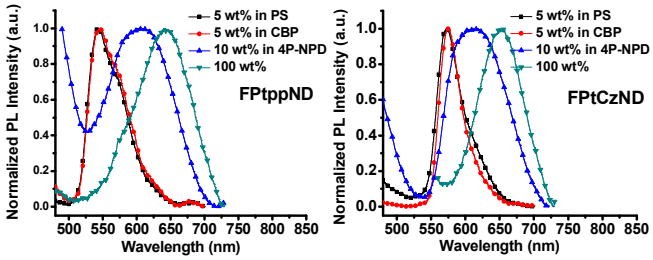

Fig. 6 Normalized PL spectra (excitation wavelength was 380 nm except for 100 wt% **FPtmmND** and **FPtOPhND** which were 420 nm) of the thin film of **FPtmmND**, **FPtOPhND**, **FPtppND** and **FPtCzND** (100 wt%) and 5 wt% **FPtXND** thin film in PS, CBP and 4P-NPD.

The PL quantum yields (Φ_{PL}) of **FPtXND** were measured in degassed dilute solution of CH_2Cl_2 by the optical dilute method with $[Ru(bpy)_3](PF_6)_2$ in acetonitrile (Φ_{PL} = 0.062) as the reference. The platinum complexes show Φ_{PL} of 0.09, 0.21, 0.08 and 0.15 for **FPtmmND**, **FPtOPhND**, **FPtppND**, and **FPtCzND**, respectively (Table 1). We note that Φ_{PL} of **FPtOPhND** is particularly higher than the rest **FPtXND** and it provides **FPtOPhND** a justified reason for high efficiency OLED, either monochromatic or hybrid white EL. In addition, the emission lifetimes (τ) were recorded for **FPtXND** complexes in degassed CH_2Cl_2 as well (see Fig. 7 for solution PL decay profile).

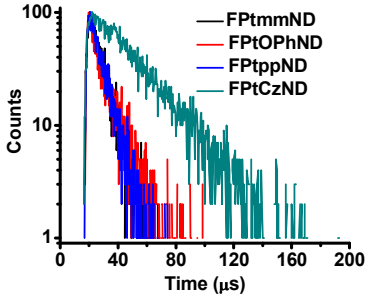

Fig. 7 Solution PL decay profile of **FPtXND**.

The platinum complexes have the emission lifetime of 5.68, 6.12, 5.61 and 25.16 μs, respectively (Table 1). All platinum complexes showed the emission lifetime in the microsecond range, suggesting that the emission originates from the ^{3}MLCT state. However, **FPtCzND** has much longer τ than other **FPtXNDs**. Based on the transient spectroscopic study of indole-substituted zinc phthalocyanine, a long-lived charge separated state due to the photoinduced electron transfer (PET) from indole to zinc phthalocyanine was observed.[18] We infer that the long τ measured for **FPtCzND** can be attributed to the twisted conformation of **CzND**, which shares the common structural feature of indole substiuent that facilates PET process generating long-lived charge separated state and long τ. Such inference is also supported by the HOMO computational study and electrochemical oxidation potential determination shown below.

Computational study

Quantum chemical calculations used DFT with the hybrid B3LYP functional and 6-31G* basis set to gain insight on the variation of HOMO/LUMO electron density distribution due to the different substituent of **FPtXND** (Fig. 8). The frontier molecular orbitals of **Alq_3** have been described previously[19] and it is known that the HOMO orbitals have significant electron density on the phenoxide side of the ligand, whereas pyridine ring makes significant contribution to the LUMO orbitals. For **FPtXND**, it is a heteroleptic platinum complex based on 8-substituted-1,5-naphthyridinolate (**XND**) and 2-(2,4-difluorophenyl)pyridine (**F**) ligands. The previously known **FPtmND** (or **FPtmmND** in the present study) exhibits the HOMO electron density mostly on the phenoxide, difluorophenyl moiety, and platinum metal ion. The LUMO electron density has a sizable contribution from methylpyridine part of **mND** (or **mmND**) and pyridine ring of **F** ligand (Fig. 8). For **FPtOPhND**, moderate electron donating phenoxy substituent affords similar contour of HOMO/LUMO to those of **FPtmND** (or **FPtmmND**). For **FPtppND**, strong electron donating piperidine substituent significantly alters the contour of HOMO by shifting electron density to piperidinopyridine ring and diminishing the electron density on difluorophenyl moiety, whereas the contour of LUMO remains similar to that of **FPtmmND**. Such computational results of **FPtppND** suggest that the lowest energy electronic transition by photoexcitation has some characteristics of ligand-to-ligand charge transfer (LLCT), which has a stronger absorption intensity than that of ^{1}MLCT or ^{3}MLCT. For **FPtCzND**, carbazolyl substituent also alters the contour of HOMO but different from that of **FPtppND**. Significant electron density was found on carbazolyl substituent according to our computation (Fig. 8). Moreover, based on the contour of HOMO and LUMO of **FPtCzND**, we can infer that the lowest energy photoexcitation involves a significant reduction of electron density on carbazolyl substituent and an increasing electron density on pyridine ring of both **ND** and **F** ligands. Such computational results are consistent with the PET proposed for **FPtCzND** in photoluminescence spectroscopic analysis shown above.

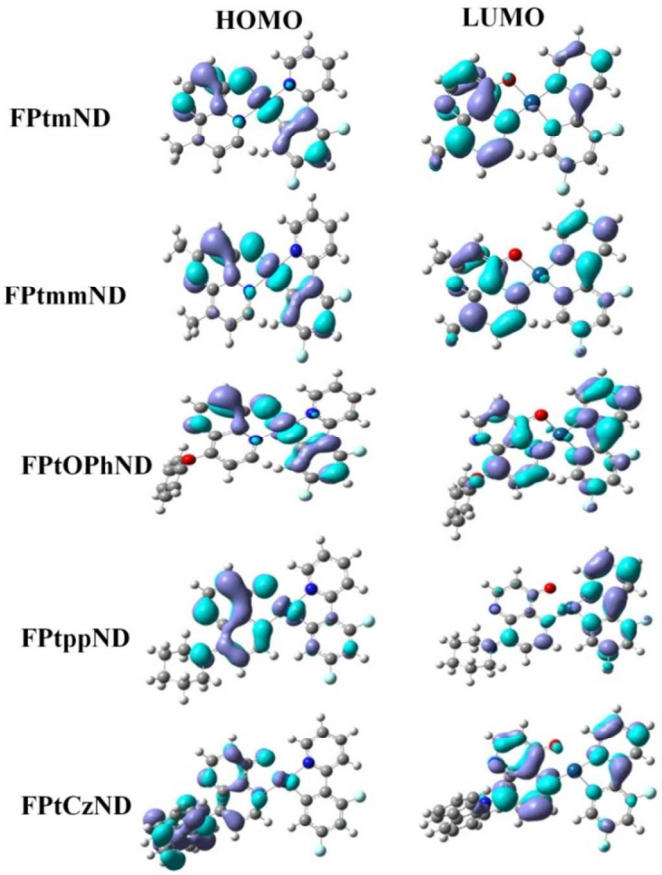

Fig. 8 Calculated electron density contour plots of HOMO (left) and LUMO (right) of the platinum complexes.

Electrochemical properties

The electrochemical properties of the platinum complexes were recorded in CH_2Cl_2 by cyclic voltammetry (CV) (see Fig. 9). Table 2 summarizes CV data obtained in this study. The energy level of HOMO of each platinum complex was determined from the first electrochemical oxidation potential (*vs.* saturated $Ag/AgNO_3$). However, due to the ill-profile of the first oxidation potential, we took the relative peak position of anodic current of ferrocene and **FPtXND** cyclic voltammograms in the calculation of HOMO energy level (Fig. 9).

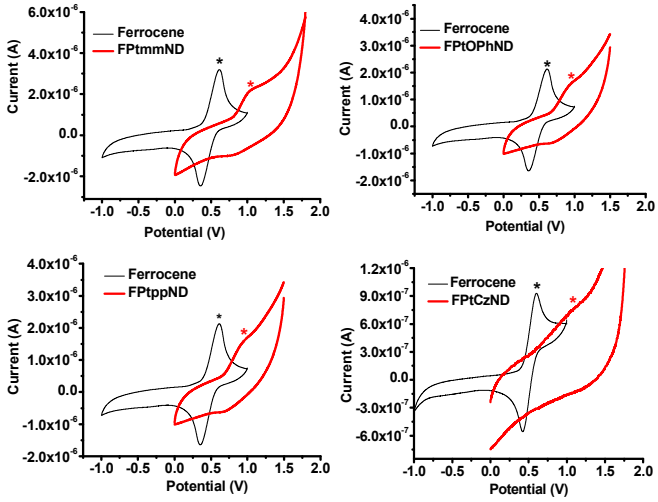

Fig. 9 Cyclic voltammograms of **FPtmmND**, **FPtOPhND**, **FPtppND**, **FPtCzND** and ferrocene (reference).

Table 2 Electrochemical data of **FPtXND**.

Pt Complexes	$E^{oxd,1}$ (V)	E_{HOMO} (eV)	λ_{onset} (nm)[a]	E_g (eV)[b]	E_{LUMO} (eV)[b]
FPtmmND	1.00	5.20	445	2.79	2.41
FPtOPhND	0.96	5.16	438	2.83	2.33
FPtppND	0.91	5.11	435	2.85	2.26
FPtCzND	1.05	5.25	473	2.62	2.63
ferrocene	0.60	-	-	-	-

[a] Determined from the onset absorption spectrum. [b] Estimated from the onset absorption spectrum by equation of $E_g = 1240/\lambda_{onset}$. [c] Deduced from the HOMO and E_g.

From the experimental results, the ease of oxidation are quite consistent with the intuition based on chemical structure of these platinum complexes. Consistent with electron donating trend of the substituent, the oxidation potential increases following order of **FPtmmND** > **FPtOPhND** > **FPtppND**. Unusually, **FPtCzND** has the highest oxidation potential among the series. This is not unreasonable because the carbazolyl substituent is electron withdrawing instead of electron donating, which is deduced from the crystal structure x-ray analysis (carbazolyl substituent has a non-π-conjugated twisted conformation to 1,5-napthyridinolate ring) and absorption/emission spectroscopy analysis in the present study. With optical energy gap (E_g) obtained from the absorption spectroscopy, HOMO and LUMO energy levels of other materials including 4,4'-bis[*N*-(1-naphthyl)-*N*-phenylamino]-biphenyl (NPB), 4P-NPD, CBP, and 1,3,5-tris(*N*-phenylbenzimidazole-2-yl)benzene (TPBI) were estimated by the same method and they are illustrated in Fig. 10.[11]

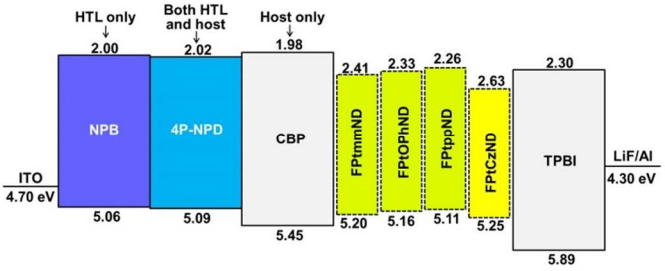

Fig. 10 Energy level alignment of materials involved in OLEDs.

Thermal properties

The thermal stabilities of platinum complexes were examined by using thermogravimetric analysis (TGA) under nitrogen atmosphere with a heating rate of 20 $^oC\ min^{-1}$. Fig. 11 and Table 1 show TGA data of platinum complexes. **FPtmmND**, **FPtOPhND**, **FPtppND** and **FPtCzND** are thermally stable with the decomposition temperature at 304, 319, 351 and 392 ^oC, respectively. These results indicate that all platinum complexes in these series are suitable for the use in OLED fabrication by vacuum-thermal-deposition process.

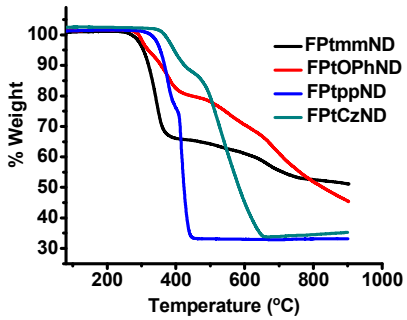

Fig. 11 Thermogravicmetric analysis (TGA) data for platinum complexes.

Electroluminescence properties

Monochromatic OLEDs

To evaluate the EL properties of **FPtmmND**, **FPtOPhND**, **FPtppND** and **FPtCzND** as potential emitters for monochromatic OLEDs, two types of device structures (Device A and B) were fabricated by vacuum-thermal-deposition process with configurations of ITO/NPB or 4P-NPD (40nm)/4,4'-*N,N'*-dicarbazolebiphenyl (CBP): *x*% **FPtXND** (20 nm)/TPBI (40 nm)/LiF(1 nm)/Al (150 nm) as shown in Fig. 12, where NPB and 4P-NPD were used as hole-transporting layer (HTL) in Device A and B, respectively. CBP was used as host material for single emitting layer (EML) and TPBI was used as electron-transporting layer (ETL). To optimize the EL performances, the dopant concentration of **FPtXND** was varied from 2 to 5 and 8 wt%.

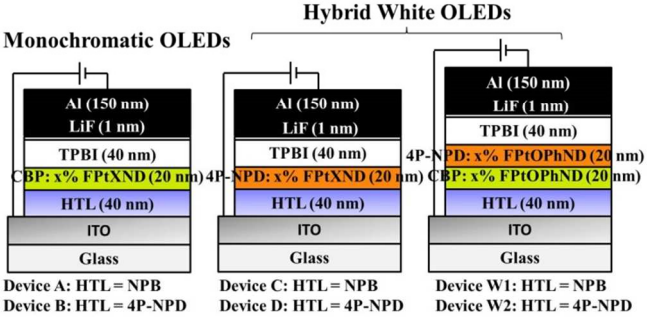

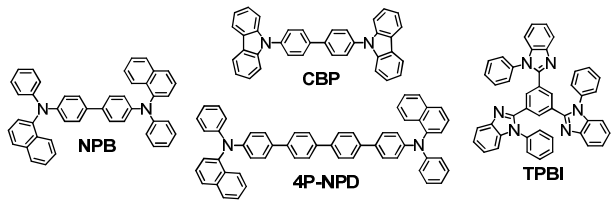

Fig. 12 The device configurations and the molecular structures of the relevant compounds used in these devices.

Some of the EL spectra and EL efficiency data of Device A and B are plotted in Fig. 13 and 14. More extensive monochromatic device data can be found in Fig. S2, S3 and S4. Containing **FPtmmND**, **FPtOPhND**, or **FPtppND** in all dopant concentration, Device A and B exhibited greenish yellow EL (λ_{max}^{EL} around 544~562 nm), which are similar to the individual PL in diluted solution (Fig. 4). Although monochromatic EL spectrum got broadening with increasing dopant concentration, both Device A and B having **FPtmmND** or **FPtOPhND** dopant displayed the optimum EL efficiency at 5 wt% dopant concentration, whereas the peak EL efficiency of Device A and B with **FPtppND** dopant were obtained at 8 wt% dopant concentration.

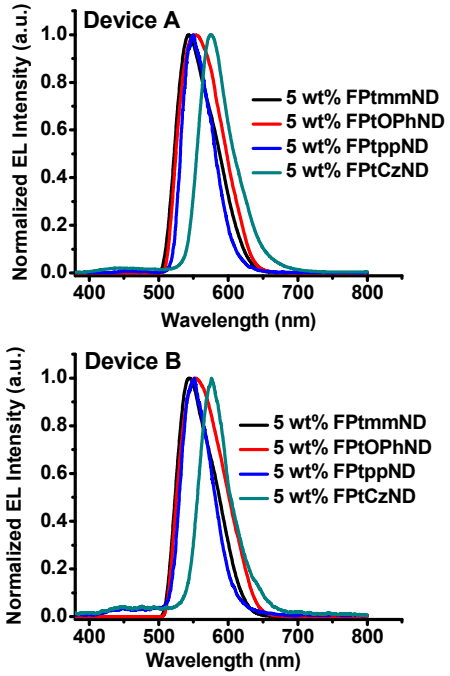

Fig. 13 Normalized EL spectra of Device A and B with different platinum complexes at 5 wt%.

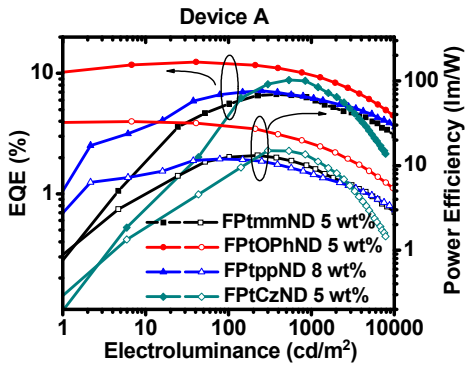

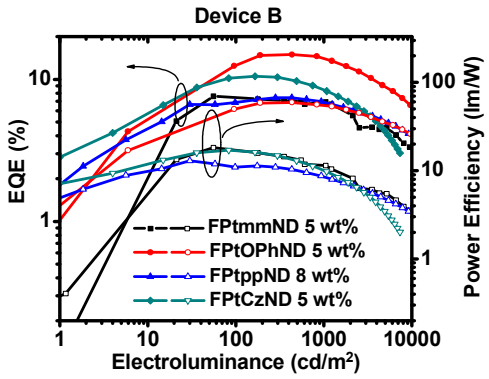

Fig. 14 External quantum efficiency and power efficiency as a function of electroluminance of monochromatic Device A (top) and Device B (bottom) at 5 wt% or 8 wt% of **FPtXND**.

Table 3 summarizes the optimized device performances using different platinum complexes as dopant materials (Device A1-4 and Device B1-4). The most efficient greenish yellow EL with $CIE_{x,y}$ (0.42-0.43, 0.57) were achieved from Device A2 and B2 having **FPtOPhND** dopant, which exhibited EL efficiencies of 12.4%, 44.8 cd A^{-1}, 33.3 lm W^{-1} and 15.0%, 59.3 cd A^{-1}, 36.7 lm W^{-1}, respectively. We attribute the high EL efficiency of Device A2 and B2 to the high Φ_{PL} 21% of **FPtOPhND**, which is the highest among four platinum complexes studied herein. When employing **FPtCzND** as dopant, orange yellow EL with $CIE_{x,y}$ (0.49-0.51, 0.47) was obtained for Device A4 and B4. Basically, such EL from **FPtCzND** OLEDs is more efficient than the greenish yellow EL of **FPtmmND** or **FPtppND** OLEDs (Table 3). In addition, having 4P-NPD as HTL, we found that Device B exhibited superior performance to those of Device A due to its higher hole mobility ($\mu_h = 6.6 \times 10^{-4}$ cm^2 V^{-1} s^{-1}) as compared to conventional NPB ($\mu_h = 3.2 \times 10^{-4}$ cm^2 V^{-1} s^{-1}).[20]

Hybrid white OLEDs

Single EML devices (Device C and D)

Hybrid white OLEDs were first fabricated with a relatively simple configuration of Device C or Device D, ITO/NPB or 4P-NPD (40 nm)/4P-NPD: *x*% **FPtXND** (20 nm)/TPBI (40 nm)/LiF(1 nm)/Al (150 nm) as shown in Fig. 12. In these devices, 4P-NPD was used as the host material for platinum complex dopant in single EML-type device. To realise an appropriate dopant concentration for WOLED devices, the dopant concentration of each platinum complex in 4P-NPD host was varied with three different concentrations of 2, 5 and 8 wt%. Fig. 15 shows the white EL spectra of Device C and D containing **FPtmmND**, **FPtOPhND**, **FPtppND**, or **FPtCzND** as dopants. More EL profiles and device performances are demonstrated in Fig. S5, S6 and S7.

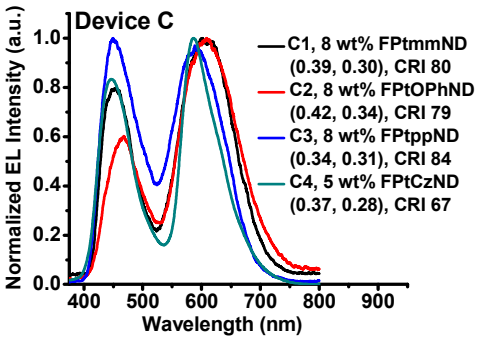

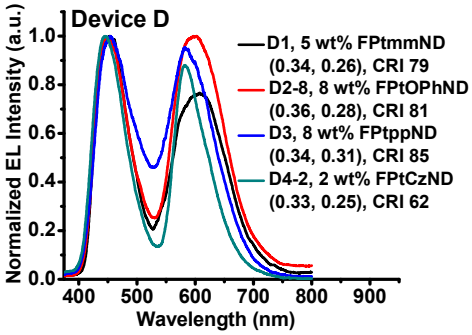

Fig. 15 Normalized hybrid white EL spectra of single EML device (Device C and D) with varied **FPtXND** dopant concentration.

Regardless of HTL, either NPB or 4P-NPD, Device C and D exhibited very different EL profiles from those of Device A and B, which are hosted by CBP. Two strong emissions were observed, containing (i) a blue emission with λ_{max}^{EL} around 430~460 nm (ii) a broad band yellow-orange-red emission with λ_{max}^{EL} around 585~610 nm. These two different emission bands can be attributed to the deep blue fluorescence from 4P-NPD host (and maybe HTL) and excimer/aggregate emission from platinum complex. Hybrid white EL with $CIE_{x,y}$ (0.34-0.39, 0.26-0.30) from **FPtmmND** OLEDs was achieved with 8 wt% dopant concentration. Device C1 and D1 displayed the peak EL efficiencies of 4.0%, 7.2 cd A^{-1}, 2.6 lm W^{-1} and 3.4%, 5.7 cd A^{-1}, 2.1 lm W^{-1}, and CRI of 80 and 79, respectively. This is nearly the only case among four platinum complexes showing better EL efficiency with NPB than 4P-NPD HTL. Considering the efficiency of white EL, **FPtmmND** has the worst performance. Once again, the best performance hybrid white EL was achieved with 8 wt% **FPtOPhND** dopant (Device D2-8 in Table 3), showing maximum EL efficiencies of 7.4%, 13 cd A^{-1}, and 6.7 lm W^{-1}. In fact, hybrid white OLED containing 2 wt% **FPtCzND** dopant (Device D4-2 in Table 3) are the second best device, although it has significantly lower CRI of 62 due to the narrow yellow-orange-red emission band of **FPtCzND** excimer/aggregate. By increasing dopant concentration (see Device D4-5 and D4-8 in Table 3), the EL efficiency of **FPtCzND** OLED can be significantly improved as high as 10.4%, 24.4 cd A^{-1}, or 11.8 lm W^{-1}, surpassing that of 8 wt% **FPtOPhND** dopant device (Device D2-8). However, Device D4-5 or D4-8 is no longer a white OLED. It showed EL with $CIE_{x,y}$ (0.45-0.57, 0.34-0.41), a yellowish white or yellow orange colour. Finally, through the variation of dopant concentration in the fabrication of **FPtOPhND** and **FPtCzND** OLEDs (Device D2-2,5,8 and Device D4-2,5,8 in Table 3), we have clearly seen the different magnitude of wavelength shifting of yellow-orange-red emission band. From 2 to 8 wt% changes of dopant concentration, there is a 30 nm red-shifting of EL due to the excimer/aggregate of **FPtOPhND**. There is only 7 nm red-shifting for **FPtCzND** devices. Such observation is very much in accordant with the different molecular packing found by x-ray crystallography. Molecules of **FPtCzND** form pair wise stacking in solid state and the number of stacking molecule is pretty much fixed at two. Whereas molecules of **FPtOPhND** form column like long stack, the number of molecule in a column stack is variable and up to dopant concentration in the thin film of the device. Nearly pure white EL $CIE_{x,y}$ (0.34, 0.31) was also achieved from **FPtppND** dopant (8 wt%) in Device C3 and D3. Both devices exhibited relatively high CRI of 84~85, which is the highest among Device C and D. It is mainly due to the additional greenish yellow emission of monomeric **FPtppND**, partially filling the spectroscopic gap between the blue emission of 4P-NPD and the yellow-orange-red emission of **FPtppND** excimer/aggregate. However, the maximum EL efficiencies of Device C3 and D3 are low (4.3%, 8.5 cd A^{-1}, and 4.1 lm W^{-1}) because of the low Φ_{PL} 8% of **FPtppND**.

Table 3 Device performances with different doping concentrations.

Device	Dopant	Dopant Conc. (wt%)	λ_{max}^{EL} (nm)	V_{on} (V)[a]	EQE (%)[b]	CE (cd A^{-1})[b]	PE (lm W^{-1})[b]	L,Voltage (cd m^{-2}) (V)[c]	CIE (x,y)[d]	CRI[e]
A1	**FPtmmND**	5	543	4.5	6.6(6.7)	27.4(27.8)	11.8(13.2)	12816(15)	(0.39,0.60)	-
B1	**FPtmmND**	5	544	4.5	7.1(7.6)	30.1(32.0)	13.4(18.3)	16863(15)	(0.39,0.60)	-
A2	**FPtOPhND**	5	551	4.0	10.8(12.4)	43.7(44.8)	22.5(33.3)	25448(15)	(0.42,0.57)	-
B2	**FPtOPhND**	5	551	4.0	14.9(15.0)	58.6(59.3)	33.1(36.7)	19386(13)	(0.43,0.57)	-
A3	**FPtppND**	8	549	5.0	6.7(7.2)	27.3(28.7)	9.9(12.0)	10337(15)	(0.40,0.57)	-
B3	**FPtppND**	8	551	4.5	7.3(7.4)	29.5(29.8)	10.0(12.9)	9232(15)	(0.38,0.57)	-
A4	**FPtCzND**	5	574	3.5	8.7(8.8)	28.3(28.6)	15.0(15.1)	7886(15)	(0.51,0.47)	-
B4	**FPtCzND**	5	576	4.0	9.8 (10.5)	31.0(33.5)	13.0(17.1)	7355(15)	(0.49,0.47)	-
C1	**FPtmmND**	8	453,614	5.0	3.9(4.0)	7.1(7.2)	2.4(2.6)	5098(15)	(0.39,0.30)	80
D1	**FPtmmND**	8	453,604	4.5	3.0(3.4)	5.0(5.7)	1.9(2.1)	5273(15)	(0.34,0.26)	79
C2	**FPtOPhND**	8	468,608	5.0	5.6(6.0)	10.0(10.5)	3.7(4.7)	7929(15)	(0.42,0.34)	79
D2-2	**FPtOPhND**	2	447,572	4.0	2.2(3.0)	2.7(3.6)	0.9(1.9)	2474(15)	(0.19,0.15)	-
D2-5	**FPtOPhND**	5	452,596	4.0	5.9(6.0)	10.4(10.5)	4.7(5.1)	8596(15)	(0.34,0.28)	80
D2-8	**FPtOPhND**	8	452,602	4.0	7.1(7.4)	12.1(13.0)	6.6(6.7)	11762(15)	(0.36,0.28)	81
C3	**FPtppND**	8	450,589	3.5	3.3(3.3)	6.7(6.7)	3.3(3.4)	4875(14.5)	(0.34,0.31)	84
D3	**FPtppND**	8	453,581	4.0	3.7(4.2)	7.7(8.5)	3.1(3.8)	4413(15)	(0.34,0.31)	85
C4	**FPtCzND**	5	447,586	4.5	5.3(5.7)	10.1(11.0)	4.4(5.1)	4965(15)	(0.37,0.28)	67
D4-2	**FPtCzND**	2	445,582	5.0	6.4(6.7)	11.7(12.3)	3.7(3.8)	3367(15)	(0.33,0.25)	62
D4-5	**FPtCzND**	5	449,583	5.0	7.5(8.1)	17.3(18.7)	5.7(6.8)	5196(15)	(0.45,0.34)	-
D4-8	**FPtCzND**	8	449,589	4.0	9.0(10.4)	20.4(23.1)	7.9(11.8)	5070(15)	(0.57,0.41)	-
W1	**FPtOPhND**	5 & 8	441,556~560	4.0	11.6(11.8)	25.5(25.9)	9.9(11.6)	10523(15)	(0.37,0.38)	87
W2	**FPtOPhND**	5 & 8	436,560,605	4.0	10.6(10.6)	18.4(18.4)	6.8(6.8)	7993(15)	(0.33,0.31)	91

[a] Turn-on voltage is the one at which the luminance over 1 cd m^{-2} was obtained. [b] The data for external quantum efficiency (EQE), current efficiency (CE), and power efficiency (PE) obtained at 500 cd/m^2. The data of peak efficiency is listed in parentheses of efficiency data. [c] Maxmium electroluminance and driving voltage. [d] Commission Internationale d'Eclairage chromaticity coordinates at 7~9 V; [e] Colour rendering index at 7~9 V.

Double EML devices (Device W1 and W2)

To improve the EL efficiency, CRI, and colour purity ($CIE_{x,y}$), devices with double EML were further fabricated, in which the platinum complex was doped into both CBP and 4P-NPD, respectively, in two-layer structure. **FPtOPhND** was selected for evaluation of WOLED performance due to its superior PL quantum yield in solution and EL efficiency in Device A, B, C, and D. Device W1 or W2 with configuration of ITO/NPB or 4P-NPD (40 nm)/CBP: 5% **FPtOPhND** (20 nm)/4P-NPD: 8% **FPtOPhND** (20 nm)/TPBI (40 nm)/LiF(1 nm)/Al (150 nm) was constructed. According to the results of monochromatic devices and WOLEDs with single EML structure, the dopant concentration of **FPtOPhND** was crucial to realise pure white OLED. The optimized dopant concentrations of **FPtOPhND** in CBP and 4P-NPD host were controlled at 5 and 8 wt%, respectively. The EL spectra of Device W1 and W2 are shown in Fig. 16, while their electroluminance dependent EL efficiencies are depicted in Fig. 16 and corresponding data are summarized in Table 3.

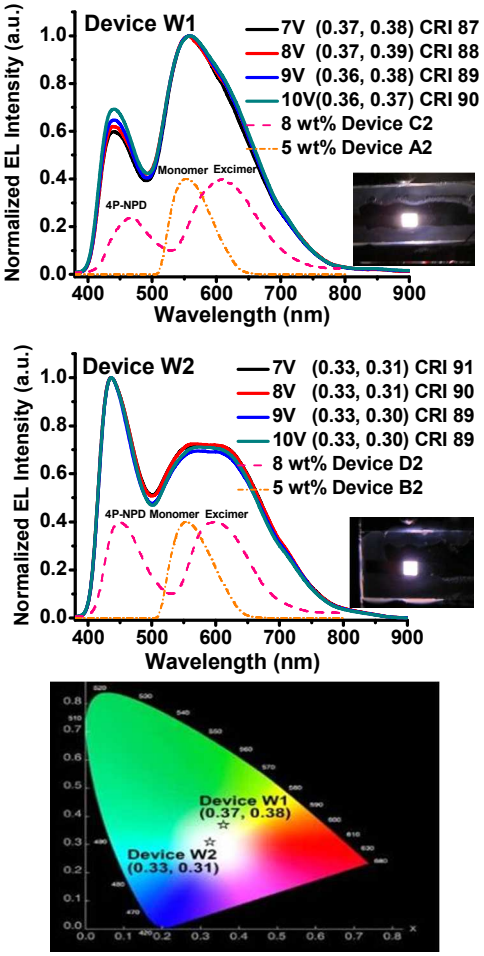

Fig. 16 Normalized hybrid white EL spectra (top and center) of double EML type-device of Device W1 and W2 at 7-10V and their CIE chromaticity diagram at 7V (bottom). The dash curves depicted in the figure are adapted from the EL spectra of Device C2, A2, D2, and B2 with the adjustment of EL intensity.

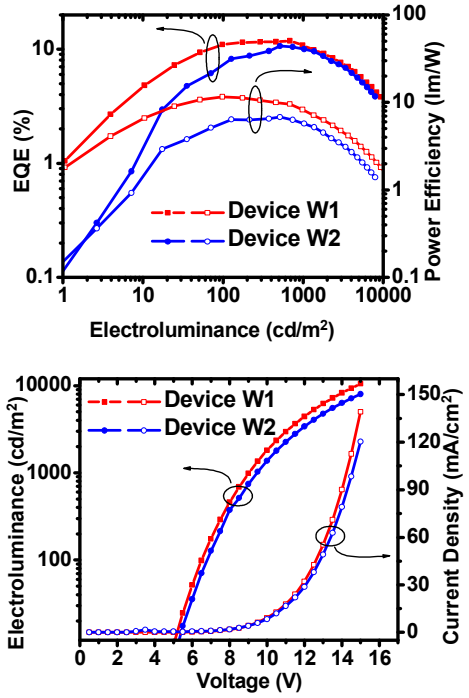

Fig. 17 External quantum efficiency and power efficiency as a function of electroluminance (top) and electroluminance-voltage-current density curves (bottom) of Device W1 and W2.

Nearly perfect white EL was acquired for both Device W1 and W2. With the contribution of greenish yellow EL from doped CBP layer, the yellow-orange-red emission band is much more broadened than before in single EML device. Since greenish yellow emission is from the isolated **FPtOPhND**, which is more EL efficient than that of excimer/aggregate, CRI, $CIE_{x,y}$ and EL efficiency are improved comprehensively. Device W1 exhibited maximum EL efficiency of 11.8%, 25.9 cd A^{-1}, and 11.6 lm W^{-1} (Fig. 17); higher CRI of 87-90 and white colour purity as $CIE_{x,y}$ (0.37, 0.38). Moreover, the EL spectra of this device were nearly same at different voltages of 7-10 V (see Fig. 16), which is due to the consistent exciton formation distributed in CBP and 4P-NPD EMLs. For Device W2, it showed even better CRI (91) and white colour purity as $CIE_{x,y}$ (0.33, 0.31) at 7 V. This is mainly due to the much increase of blue fluorescence and moderate increase of greenish yellow phosphorescence in EL spectra. Moreover, similar to Device W1, Device W2 exhibited consistent white EL spectroscopic profile, which is essentially voltage independent. However, due to the less efficiency nature of fluorescence-based EL, somewhat lower peak EL efficiency of 10.6%, 18.4 cd A^{-1}, or 6.8 lm W^{-1} was obtained by Device W2. Nevertheless, double EML and single phosphorescence dopant devices, Device W1 and W2, exhibit high CRI~90 and much better EL efficiency and colour stability, when compared with those hybrid white OLED based on platinum complexes reported in literature.[9,10]

Conclusions

In summary, four new functionalized platinum complexes with dimethyl, phenoxy, piperidino or carbazol substituent on 4-hydroxy-1,5-naphthyridine were synthesized and fully characterized. Their PL revealed that, in addition to greenish yellow or orange yellow emission in diluted solution, the platinum complexes also exhibited an excimer/aggregate emission (red-shifted wavelength) in a

concentrated solution or in thin film. PHOLEDs were constructed based on these platinum complexes. By employing CBP as host, the monochromatic greenish yellow or orange yellow EL were obtained with the maximum efficiencies of 15.0%, 59.3 cd A^{-1}, 36.7 lm W^{-1} for **FPtOPhND** and 10.5%, 33.5 cd A^{-1}, 17.1 lm W^{-1} for **FPtCzND**, respectively. Upon switching the host material to 4P-NPD, fluorescence-phosphorescence hybrid white OLEDs with a single emitting layer were achieved. Whereas **FPtppND** provided the highest CRI of 84~85, It was **FPtOPhND** showing highest white EL efficiency, external quantum efficiency of 7.4%, current efficiency of 13.0 cd A^{-1}, or power efficiency of 6.7 lm W^{-1}. They are even better than those of **FPtmND** reported previously.[11] With a double emitting layer design of hybrid white OLED, the performance of **FPtOPhND** OLED has been improved comprehensively. Nearly perfect white EL having $CIE_{x,y}$ (0.33, 0.31) was achieved with high efficiency (10.6%, 18.4 cd A^{-1}, and 6.8 lm W^{-1}) and very high CRI of 91. Moreover, such white EL has little changes on both CRI and $CIE_{x,y}$ when the driving voltage varied between 7 and 10 V. These results clearly demonstrate the great potential of hybrid white OLED having double emitting layer design together with blue fluorescent host and dual phosphorescence from single platinum complex dopant for display and lighting applications.

Experimental Section

General information

Photoluminescence (PL) spectra were recorded on a Hitachi fluorescence spectrophotometer F-4500, and the same spectrophotometer was used to record the EL spectra of OLEDs. UV-visible electronic absorption spectra were recorded on a Hewlett-Packard 8453 Diode Array spectrophotometer. The ^1H and ^{13}C NMR spectra were recorded on a Bruker AMX-400 MHz, AVA-400 MHz or Bruker AV-500 MHz Fourier-transform spectrometer at room temperature. Elemental analyses (on a Perkin-Elmer 2400 CHN Elemental Analyzer) and electrospray ionization (ESI) or matrix-assisted laser desorption/ionization time-of-flight (MALDI-TOF) mass spectra (on a VA Analytical 11-250J or 4800 MALDI TOF/TOF Analyzer) were recorded by the Elemental Analyses and Mass Spectroscopic Laboratory in-house service of the Institute of Chemistry, Academic Sinica. Thermogravimetric analyse was performed under nitrogen with a Perkin-Elmer TGA-7 TG analyzer.

Luminescence lifetime was determined on an Edinburgh FL920 time-correlated pulsed single-photon-counting instrument. The phosphorescence emission was detected at 90° via a second Czerny-Turner design monochromator onto a thermoelectrically cooled red-sensitive photomultiplier tube. The resulting photon counts were stored on a microprocessor-based multichannel analyzer. The instrument response function was profiled using a scatter solution and subsequently deconvoluted from the emission data to yield an undisturbed decay. Nonlinear least squares fitting of the PL decay curves were performed with the Levenburg-Marquardt algorithm and implemented by the Edinburgh Instruments F900 software.

Emission quantum yields (Φ_{PL}) in degassed CH_2Cl_2 were determined with $[Ru(bpy)_3](PF_6)_2$ (bpy = 2,2'-bipyridine) in acetonitrile as a reference ($\Phi_{PL} = 0.062$)[21] and calculated according to the following equation: $\Phi_s = \Phi_r(B_r/B_s)(n_s/n_r)^2(D_s/D_r)$, where the subscripts *s* and *r* refer to sample and reference standard solution respectively, *n* is the refractive index of the solvents, *D* is the integrated intensity, and Φ is the luminescence quantum yield. The quantity *B* was calculated by $B = 1 - 10^{-AL}$, where A is the absorbance at the excitation wavelength and L is the optical path length. The solid-state (PS thin film) PL quantum yields of the platinum complexes were determined by the integrating-sphere method.[22,23]

Redox potentials of the compounds were determined by cyclic voltammetry (CV) using a BAS 100B electrochemical analyzer with a scanning rate at 100 mV/s. The interested compounds were dissolved in deoxygenated dry CH_2Cl_2 with 0.1 M tetrabutylammonium perchlorate as the electrolyte. We used a platinum working electrode and a saturated nonaqueous $Ag/AgNO_3$ referenced electrode. Ferrocene was used for potential calibration (all reported potentials are referenced against Ag/Ag^+) and for reversibility criteria. Energy level of ferrocene (4.8 V below the vacuum level) is used as the reference.[24] The HOMO energy levels were calculated with empirical relation $E_{HOMO} = -e[(E^{oxd,1} - E_{(ferrocene)}) + 4.8]$ eV.

X-Ray Crystallography Studies

Data collection was carried out on a Brucker X8APEX CCD diffractometer at 100 K for **FPtOPhND** and **FPtCzND** single crystals. The radiation of Mo radiation (λ = 0.71073 Å) was used for both crystals. The unit cell parameters were obtained by a least-square fit to the automatically centered settings for reflections. Intensity data were collected by using the $\omega/2\theta$ scan mode. Corrections were made for Lorentz and polarization effects. The structures were solved by direct methods *SHELX-97*.[25] All non-hydrogen atoms were located from the difference Fourier maps and were refined by full-matrix least-squares procedures. The position of hydrogen atoms was calculated and located. Calculations and full-matrix least-squares refinements were performed utilizing the *WINGX* program package[26] in the evaluation of values of *R* (F_o) for reflections with $I > 2\sigma(I)$ and R_w (F_o), where $R = \Sigma||F_o| - |F_c||/\Sigma|F_o|$ and $R_w = [\Sigma\{w(F_o^2 - F_c^2)^2\}/\Sigma\{w(F_o^2)^2\}]^{1/2}$. Intensities were corrected for absorption.

OLED device fabrication and measurements

OLED devices were fabricated by thermal vacuum deposition. The substrate was an indium-tin-oxide (ITO) coated glass (Merck Display Technology, Taiwan) with a sheet resistance of < 30 Ω/sq. ITO-coated glass substrates were cleaned with detergent, deionized water, acetone, and isopropanol, followed by oxygen plasma treatment. The current density–voltage–luminance characteristics of the devices were measured using a Keithley 2400 source meter and a Newport 1835C optical meter equipped with a Newport 818-ST silicon photodiode, respectively. The device was placed close to the photodiode such that all the forward light entered the photodiode. The effective size of the emitting diodes was 4.00 mm^2, which is significantly smaller than the active area of the photodiode detector, a condition known as "under-fillling", satisfying the measurement protocol.[27] This is one of the most conventional ways in measuring the EL efficiency of OLEDs, although sometimes experimental errors may arise due to the non-Lambertian emission of OLEDs. The colour rendering index (CRI) of white OLEDs was measured by a spectroradiometer (Specbos 1201, JETI Technishe Instrumente GmbH).

Materials

For the materials used in device fabrication, NPB,[28] CBP,[29] TPBI,[30] 2-(2,4-difluorophenyl)pyridine (**F**)[31] and 4P-NPD[11] were prepared via published methods. All materials were purified by vacuum train sublimation before the usage in device fabrication. Synthetic precursors **1** and **2**, 3-nitropyridine derivatives ($\mathbf{3_{OPh}}$, $\mathbf{3_{pp}}$, and $\mathbf{3_{Cz}}$), and 3-pyridiylamine derivatives ($\mathbf{4_{OPh}}$, $\mathbf{4_{pp}}$, and $\mathbf{4_{Cz}}$) were prepared by adopting the synthetic protocols reported in literatures with slight modification as shown in ESI. The Pt μ-dichloro-bridged dimer $\mathbf{(FPtCl)_2}$ was prepared following literature procedures.[32] All reactions were performed under nitrogen. Solvents were carefully dried and distilled from appropriate drying agents prior to use. The

syntheses of ligands and platinum complexes are summarized in Scheme 2. The detailed procedure and structural characterization data of the new compounds are shown below.

General synthesis procedure of pre-XND.

To a mixture of 4-substituted pyridine-3-amine $\mathbf{4_{OPh}}$, $\mathbf{4_{pp}}$, or $\mathbf{4_{Cz}}$ (1 equivalent) and Meldrum's acid 2,2-dimethyl-[1,3]dioxane-4,6-dione (1.2 equivalent) was added triethyl orthoformate or triethyl orthoacetate (6 equivalent). The mixture was then heated at reflux under nitrogen for 4 h. After cooling to room temperature, the reaction mixture was removed by vacuum distillation. The resulting solid was purified by flash column chromatography (silica gel, ethyl acetate/dichloromethane: 1/1) to afford the intermediate **pre-XND**.

2,2-Dimethyl-5-(1-(4-methylpyridin-3-ylamino)ethylidene)-1,3-dioxane-4,6-dione (pre-mmND). The specific amounts of chemicals used: 3-amino-4-methylpyridine (2.0 g, 18.5 mmol), Meldrum's acid (3.2 g, 22.2 mmol) and triethyl orthoacetate (18.0 g, 111.0 mmol). The product (**pre-mmND**) was obtained as a pale yellow solid (3.8 g, 75%). ^{1}H NMR (400 MHz, $CDCl_3$): δ 12.73 (s, 1H), 8.52 (d, 1H, J = 4.80 Hz), 8.39 (s, 1H), 7.30 (d, 1H, J = 4.96 Hz), 2.50 (s, 3H), 2.31 (s, 3H), 1.76 (s, 6H). ^{13}C NMR (100 MHz, $CDCl_3$): δ 173.98, 167.60, 162.53, 149.50, 147.67, 143.81, 132.54, 125.75, 103.02, 86.48, 26.63, 19.43, 17.33. FAB-MS: calcd. 276.11, m/z = 277.1 (M+H$^+$).

5-((2-Phenoxyphenylamino)methylene)-2,2-dimethyl-1,3-dioxane-4,6-dione (pre-OPhND). The specific amounts of chemicals used: 4-phenoxypyridin-3-amine (**3a**) (2.0 g, 10.7 mmol), Meldrum's acid (1.9 g, 13.2 mmol) and triethyl orthoformate (9.6 g, 64.8 mmol). The product (**pre-OPhND**) was obtained as a white solid (2.8 g, 77%). ^{1}H NMR (400 MHz, $CDCl_3$): δ 11.48 (d, 1H, J = 13.80 Hz), 8.75 (d, 1H, J = 14.24 Hz), 8.64 (s, 1H), 8.29 (d, 1H, J = 5.52 Hz), 7.46 (t, 2H, J = 7.82 Hz), 7.31 (t, 1H, J = 7.38 Hz), 7.13 (d, 2H, J = 8 Hz), 6.68 (d, 1H, J = 5.56 Hz), 1.73 (s, 6H). ^{13}C NMR (100 MHz, $CDCl_3$): δ 165.27, 163.19, 154.97, 153.05, 152.27, 148.74, 139.34, 130.45, 126.33, 125.44, 120.79, 110.27, 105.30, 88.95, 27.12. FAB-MS: calcd. 340.1, *m/z* = 341.1 (M+H$^+$).

5-((2-(Piperidin-1-yl)phenylamino)methylene)-2,2-dimethyl-1,3-dioxane-4,6-dione (pre-ppND). The specific amounts of chemicals used: 4-(piperidin-1-yl)pyridin-3-amine (**3b**) (1.5 g, 8.5 mmol), Meldrum's acid (1.5 g, 10.4 mmol) and triethyl orthoformate (7.5 g, 50.6 mmol). The product (**pre-ppND**) was obtained as a white solid (1.6 g, 57%). ^{1}H NMR (400 MHz, $CDCl_3$): δ 11.32 (d, 1H, J = 13.24 Hz), 8.73 (d, 1H, J = 14.32 Hz), 8.50 (s, 1H), 8.35 (d, 1H, J = 5.24 Hz), 6.96 (d, 1H, J = 5.32 Hz), 2.91 (t, 4H, J = 5.24 Hz), 1.81 (m, 4H), 1.72 (s, 6H), 1.60 (t, 2H, J = 5.76). ^{13}C NMR (100 MHz, $CDCl_3$): δ 165.21, 163.30, 151.17, 148.59, 138.56, 128.82, 114.83, 105.13, 88.15, 52.30, 27.05, 25.66, 23.77. FAB-MS: calcd. 331.15, *m/z* = 332.2 (M+H$^+$).

5-((4-(9H-Carbazol-9-yl)pyridin-3-ylamino)methylene)-2,2-dimethyl-1,3-dioxane-4,6-dione (pre-CzND). The specific amounts of chemicals used: 4-(9H-carbazol-9-yl)pyridin-3-amine (**3c**) (2.0 g, 7.7 mmol), Meldrum's acid (1.3 g, 9.0 mmol) and triethyl orthoformate (6.9 g, 46.6 mmol). The product (**pre-CzND**) was obtained as a white solid (2.1 g, 66%). ^{1}H NMR (400 MHz, $CDCl_3$): δ 10.87 (d, 1H, J = 13.6 Hz), 9.00 (s, 1H), 8.75 (d, 1H, J = 5.2 Hz), 8.55 (d, 2H, J = 13.6 Hz), 8.17 (d, 1H, J = 5.2 Hz), 7.57 (d, 1H, J = 5.2 Hz), 7.44 (t, 2H, J = 7.6 Hz), 7.36 (t, 2H, J = 7.6 Hz), 7.11 (d, 2H, J = 7.6 Hz), 1.57 (s, 6H).^{13}C NMR (100 MHz, $CDCl_3$) δ 164.40, 162.75, 152.06, 150.32, 148.59, 141.08, 139.30, 136.31, 132.23, 126.70, 124.54, 123.60, 121.71, 121.12, 109.36, 106.62, 105.25, 89.91, 26.98. EI-MS: calcd. 413.14, m/z = 413.10 (M$^+$).

General synthesis procedure of XND ligands.

Compound **pre-XND** (1~2 g) in diphenyl ether (35 mL) was heated at 260 ^{o}C and stirred under nitrogen atmosphere for 10-60 min. During the reaction, the colour of the solution changed from orange yellow to dark brown or black. After cooling to room temperature, the reaction solution was filtered to isolate solid product. The solid was rinsed with diphenyl ether and subjected to purification by zone-temperature sublimation.

4-Hydroxy-2,8-dimethyl-1,5-naphthyridine (mmND). The specific amounts of chemicals used: **pre-mmND** (2 g, 7.2 mmol). The product was obtained as a white solid (0.9 g, 71%)**.** ^{1}H NMR (400 MHz, CD_3OD): δ 8.52 (d, 1H, J = 4.48 Hz), 7.51 (d, 1H, J = 4.8 Hz), 6.34 (s, 1H), 2.62 (s, 3H), 2.52 (s, 3H). ^{13}C NMR (100 MHz, CD_3OD): δ 153.52, 147.39, 139.95, 139.08, 137.65, 128.73, 112.49, 20.05, 17.31. EI-MS: calcd. 174.08, *m/z* = 174.08 (M$^+$).

4-Hydroxy-8-phenoxy-1,5-naphthyridine (OPhND). The specific amounts of chemicals used: **pre-OPhND** (2.5 g, 7.4 mmol). The product was obtained as a white solid (1.1 g, 63%)**.** ^{1}H NMR (400 MHz, CD_3OD): δ 8.51 (d, 1H, J = 5.12 Hz), 8.02 (d, 1H, J = 7.28 Hz), 7.58 (t, 2H, J = 6.28 Hz), 7.41 (t, 1H, J = 7.34 Hz), 7.32 (d, 2H, J = 8.24 Hz), 6.89 (d, 1H, J = 5.28 Hz), 6.57 (d, 1H, J = 7.24 Hz). ^{13}C NMR (100 MHz, CD_3OD): δ 179.28, 157.41, 154.82, 148.83, 142.63, 141.08, 131.80, 130.68, 127.73, 122.15, 113.15, 110.59. EI-MS: calcd. 238.07, *m/z* = 238.07 (M$^+$).

4-Hydroxy-8-piperidino-1,5-naphthyridine (ppND). The specific amounts of chemicals used: **pre-ppND** (1.5 g, 4.5 mmol). The product was obtained as a pale yellow solid (0.5 g, 48%)**.** ^{1}H NMR (400 MHz, CD_3OD): δ 8.47 (br, 1H), 8.04 (d, 1H, J = 6.88 Hz), 7.27 (d, 1H, J = 4.28 Hz), 6.53 (d, 1H, J = 6.96 Hz), 1.89 (m, 4H), 1.73 (m, 2H). ^{13}C NMR (125 MHz, CD_3OD): δ 155.19, 147.67, 147.22, 143.06, 134.49, 116.26, 115.81, 112.81, 54.07, 26.92, 25.25. EI-MS: calcd. 229.12, m/z = 229.12 (M$^+$).

4-Hydroxy-8-carbazol-1,5-naphthyridine (CzND). The specific amounts of chemicals used: **pre-CzND** (2.0 g, 4.8 mmol). The product was obtained as a brown solid (0.7 g, 46%)**.** ^{1}H NMR(400 MHz, CD_3OD) : δ 8.94 (d, 1H, J = 4.8 Hz), 8.24 (d, 2H, J = 8.0 Hz), 7.85 (d, 1H, J = 4.8 Hz), 7.44 (t, 2H, J = 7.8 Hz), 7.37 (t, 2H, J = 7.6 Hz), 7.12 (d, 2H, J = 8.0 Hz), 6.61 (d, 2H, J = 7.2 Hz). ^{13}C NMR (125 MHz, CD_3OD): δ 179.13, 164.96, 159.14, 157.56, 148.90, 145.86, 144.55, 144.39, 144.12, 142.29, 139.30, 130.89, 127.85, 126.94, 126.06, 123.01, 122.46, 121.77, 113.30, 111.09. EI-MS: calcd. 311.1, m/z= 311.1 (M$^+$).

General procedure for synthesis of FPtXND complexes.

The Pt complex $\mathbf{(FPtCl)_2}$ were prepared following literature procedures.[26] The K_2PtCl_4 and 2.5 equivalent of **F** ligand were mixed in a 3:1 mixture of 2-ethoxyethanol and water. The mixture was heated to 80 ^{o}C for 16 h. The desired $\mathbf{(FPtCl)_2}$ were precipitated in the water. The resulting yellow-greenish powder was filtered and was subsequently reacted with **XND** ligand without further purification. A stirred mixture of $\mathbf{(FPtCl)_2}$ (1 equivalent), Na_2CO_3 (10 equivalent) and **XND** ligand (2.1 equivalent) in 2-ethoxyethanol was heated to 80 ^{o}C for 16 h. After cooling, the solution was concentrated under reduced pressure. The resultant residue was subjected to column chromatography (silica gel, CH_2Cl_2/MeOH 15:1(v/v)) to afford product.

FPtmmND. The specific amounts of chemicals used: **$(FPtCl)_2$** (0.150 g, 0.18 mmol), Na_2CO_3 (0.190 g, 1.80 mmol) and **mmND** (0.066 g, 0.38 mmol). The product was obtained as a yellow solid (0.120 g, 60%). ^{1}H NMR (400 MHz, CD_3Cl): δ 9.28 (d, 1H, J = 5.36 Hz), 8.73 (d, 1H, J = 5.40 Hz), 7.97 (d, 1H, J = 8.24 Hz), 7.86 (t, 1H, J = 7.80 Hz), 7.42 (d, 1H, J = 5.32 Hz), 7.17 (t, 1H, J = 6.46 Hz), 6.96 (dd, 1H, J = 9.48 Hz), 6.71 (s, 1H), 6.62 (td, 1H, J = 10.46 Hz), 2.78 (s, 3H), 2.62 (s, 3H). ^{13}C NMR (100 MHz, CD_3Cl): δ 162.79, 150.54, 149.40, 144.69, 139.15, 125.65, 124.30, 122.01, 121.81, 121.46, 114.35, 112.21, 99.64, 99.38, 99.11, 30.91, 25.39, 17.46. HR-ESI-MS: calcd. 558.08, m/z = 558.08 (M^+). Anal. Found (calcd) for $C_{21}H_{15}F_2N_3OPt$: C 44.63 (45.17), H 2.78 (2.71), N 7.25 (7.52).

FPtOPhND. The specific amounts of chemicals used: **$(FPtCl)_2$** (0.170 g, 0.20 mmol), Na_2CO_3 (0.214 g, 2.00 mmol) and **OPhND** (0.101 g, 0.42 mmol). The product was obtained as an orange-red solid (0.190 g, 76%). ^{1}H NMR (400 MHz, CD_3Cl): δ 9.11 (d, 1H, J = 5.36 Hz), 8.51 (t, 2H, J = 5.60 Hz), 7.84 (m, 2H), 7.54 (t, 2H, J = 7.60 Hz), 7.38 (m, 3H), 7.07 (t, 1H, J = 6.00 Hz), 6.80 (d, 1H, J = 5.20 Hz), 6.70 (d, 1H, J = 9.6 Hz), 6.61 (d, 1H, J = 6 Hz), 6.54 (t, 1H, J = 10.4 Hz). ^{13}C NMR (100 MHz, CD_3Cl): δ 173.43, 163.86, 163.39, 163.32, 153.59, 153.43, 149.29, 147.90, 146.93, 138.93, 130.53, 129.43, 128.80, 126.57, 121.63, 114.06, 113.89, 113.22, 106.70, 99.51, 99.24, 98.98. HR-ESI-MS: calcd. 622.08, m/z = 623.09 ($M+H^+$). Anal. Found (calcd) for $C_{25}H_{15}F_2N_3O_2Pt$: C 48.56 (48.24), H 2.50 (2.43), N 6.62 (6.75).

FPtppND. The specific amounts of chemicals used: **$(FPtCl)_2$** (0.150 g, 0.18 mmol), Na_2CO_3 (0.190 g, 1.80 mmol) and **ppND** (0.086 g, 0.38 mmol). The product was obtained as a yellow solid (0.087 g, 47%). ^{1}H NMR (400 MHz, CD_3Cl): δ 9.28 (d, 1H, J = 5.36 Hz), 8.48 (d, 1H, J = 6.40 Hz), 8.27 (d, 1H, J = 5.24 Hz), 7.93 (d, 1H, J = 8.04 Hz), 7.80 (t, 1H, J = 7.58 Hz), 7.11 (t, 1H, J = 6.34 Hz), 6.94 (d, 1H, J = 9.08 Hz), 6.77 (d, 1H, J = 5.28 Hz), 6.70 (d, 1H, J = 6.40 Hz), 6.58 (t, 1H, J = 9.82 Hz), 3.99 (br, 4H), 1.79 (br, 6H). ^{13}C NMR (100 MHz, CD_3Cl): δ 173.40, 164.08, 163.95, 163.55, 163.48, 161.54, 161.42, 159.22, 155.65, 149.36, 149.27, 147.04, 146.01, 143.33, 143.27, 139.54, 138.74, 129.54, 122.03, 121.84, 121.44, 114.55, 114.35, 112.04, 106.78, 99.31, 99.05, 98.78, 51.51, 25.88, 24.64. HR-ESI-MS: calcd. 613.13, m/z = 613.13 (M^+). Anal. Found (calcd) for $C_{24}H_{20}F_2N_4OPt$: C 46.81 (46.98), H 3.22 (3.29), N 9.01 (9.13).

FPtCzND. The specific amounts of chemicals used: **$(FPtCl)_2$** (0.150 g, 0.18 mmol), Na_2CO_3 (0.190 g, 1.80 mmol) and **CzND** (0.117 g, 0.38 mmol). The product was obtained as an orange solid (0.162 g, 65%). ^{1}H NMR (400 MHz, CD_3Cl): δ 9.38 (d, 1H, J = 5.60 Hz), 9.12 (d, 1H, J = 5.60 Hz), 8.47 (d, 1H, J = 5.60 Hz), 8.13 (d, 2H, J = 7.60 Hz), 8.06 (d, 1H, J = 8.00 Hz), 7.91 (m, 2H), 7.40 (m, 6H), 7.23 (m, 1H), 7.03 (dd, 1H, J = 9.20 Hz), 6.95 (d, 1H, J = 5.20 Hz), 6.68 (td, 1H, J = 9.20 Hz). ^{13}C NMR (125 MHz, CD_3Cl): δ 174.27, 164.01, 161.82, 161.74, 161.63, 159.67, 159.57, 155.06, 149.74, 149.13, 147.03, 146.51, 142.67, 142.06, 140.82, 139.77, 129.92, 126.35, 125.28, 122.43, 122.27, 121.95, 121.71, 120.59, 114.66, 114.51, 113.58, 111.87, 100.22, 100.01, 99.79 HR-ESI-MS: calcd. 695.11, m/z = 696.12 ($M+H^+$). Anal. Found (calcd) for $C_{31}H_{18}F_2N_4OPt$: C 53.34 (53.53), H 2.61 (2.61), N 8.15 (8.05).

Acknowledgements

We thank the Ministry of Science and Technology (NSC 101-2113-M-001-004-MY2), Taiwan International Graduate Program (TIGP) of Academia Sinica, Academia Sinica, and National Taiwan University for financial support. We also want to thank Dr. Yung-Ting Chang for the measurement of emission quantum yields of samples in thin film.

References

1. (*a*) M A. Baldo, M. E. Thomson and S. R. Forrest, *Nature*, 2000, **403**, 750; (*b*) B. W. D' Andrade and S. R. Forrest, *Adv. Mater.*, 2004, **16**, 1585; (*c*) S. Chen, L. Deng, J. Xie, L. Xie, Q. Fan and W. Huang, *Adv. Mater*., 2010, **22**, 5227; (*d*) H. Sasabe and J. Kido, *Chem. Mater*., 2011, **23**, 621; (*e*) K. S. Yook and J. Y. Lee, *Adv. Mater*., 2012, **24**, 3169; (*f*) Y. L. Chang, B. A. Kamino, Z. Wang, M. G. Helander, Y. Rao, L. Chai, S. Wang, T. P. Bender and Z. H. Lu, *Adv. Funct. Mater*., 2013, **23**, 3204.
2. (*a*) S. Reineke , F. Lindner , G. Schwartz , N. Seidler , K. Walzer , B. Lüssem, K. Leo, *Nature*, 2009 , **459** , 234; (*b*) H. Sasabe, J.-I. Takamatsu, T. Motoyama, S. Watanabe, G. Wagenblast, N. Langer, O. Molt, E. Fuchs, C. Lennartz and J. Kido, *Adv. Mater*., 2010, **22**, 5003.
3. J. S. Swensen, E. Polikarpov, A. V. Ruden, L. Wang, L. S. Sapochak and A. B. Padmaperuma, *Adv. Funct. Mater*., 2011, **21**, 3250.
4. (*a*) X.-M. Yu, G.-J. Zhou, C.-S. Lam, W.-Y. Wong, X.-L. Zhu, J.-X. Sun, M. Wong, H.-S. Kwok, *J. Organomet. Chem.*, 2008, **693**, 1518; (*b*) S.-L. Lai, W.-Y. Tong, S. C. F. Kui, M.-Y. Chan, C.-C. Kwok and C.-M. Che, *Adv. Funct. Mater.*, 2013, **23**, 5168; (*c*) J. Li, R. Wang, R. Yang, W. Zhou and X. Wang, *J. Mater. Chem. C*, 2013, **1**, 4171.
5. (*a*) X.-M. Yu, H.-S. Kwok, W.-Y. Wong and G.-J. Zhou, *Chem. Mater*., 2006, **18**, 5097; (*b*) Q. Wang, J. Ding, D. Ma, Y. Cheng, L. Wang, X. Jing and F. Wang, *Adv. Funct. Mater*., 2009, **19**, 84; (*c*) R. Wang, D. Liu, R. Zhang, L. Deng and J. Li, *J. Mater. Chem*., 2012, **22**, 1411; (*d*) C.-H. Chang, C.-L. Ho, Y.-S. Chang, I.-C. Lien, C.-H. Lin, Y.-W. Yang, J.-L. Liao and Y. Chi, *J. Mater. Chem. C*, 2013, **1**, 2639.
6. Y. Sun, N. C. Giebink, H. Kannol, B. Ma, M. E. Thompson and S. R. Forrest, *Nature*, 2006, **440**, 908.
7. (*a*) G. Schwartz, M. Pfeiffer, S. Reineke, K. Walzer and K. Leo, *Adv. Mater.*, 2007, **19**, 3672. (*b*) G. Schwartz, S. Reineke, K. Walzer and K. Leo, *Appl. Phys. Lett.*, 2008, **92**, 053311. (*c*) G. Schwartz, S. Reineke, T. C. Rosenow, K. Walzer and K. Leo, *Adv. Funct. Mater.*, 2009, **19**, 1319. (*d*) T. C. Rosenow, M. Furno, S. Reineke, S. Olthof, B. Lussem and K Leo, *J. Appl. Phys.* 2010, **108**, 113113. (*e*) S. Hofmann, T. C. Rosenow, M. C. Gather, B. Lussem and K Leo, *Phys. Rew. B* **2012**, **85**, 245209.
8. (*a*) W.-Y. Hung, L.-C. Chi, W.-J. Chen, Y.-M. Chen, S.-H. Chou and K.-T. Wong, *J. Mater. Chem.*, 2010, **20**, 10113; (*b*) J. Wan, C.-J. Zheng, M.-K. Fung, X.-K. Liu, C.-S. Lee and X.-H. Zhang, *J. Mater. Chem.,* 2012, **22**, 4502; (*c*) J. Ye, C.-J. Zheng, X.-M. Ou, X.-H. Zhang, M.-K. Fung and C.-S. Lee, *Adv. Mater*., 2012, **24**, 3410; (*d*) S. Hofmann, M. Furno, B. Lussem, K. Leo and M. C. Gather, *Phys. Status Solidi A*, 2013, **210**, 1467.
9. (*a*) C.-M. Che, S.-C. Chan, H.-F. Xiang, M. C. Chan, Y. Liu and Y. Wang, *Chem. Commun.* **2004**, 1484; (*b*) B.-P. Yang, C. C. C. Cheung, S. C. F. Kui, H.-F. Xiang, V. A. L. Roy, S.-J. Xu and C.-M. Che, *Adv. Mater.*, 2007, **19**, 3599; (*c*) G. Zhou, Q. Wang, X. Wang, C.-L. Ho, W.-Y. Wong, D. Ma, L. Wang and Z. Lin, *J. Mater. Chem.*, 2010, **20**, 7472.
10. (*a*) E. Rossi, L. Murphy, P. L. Brothwood, A. Colombo, C. Dragonetti, D. Roberto, R. Ugo, M. Cocchi and J. A. G. Williams, *J. Mater. Chem*., 2011, **21**, 15501; (*b*) L. Murphy, P. Brulatti, V. Fattori, M. Cochi and J. A. G. Williams, *Chem. Commun*., 2012, **48**, 5817; (*c*) E. Rosssi, A. Colombo, C. Dragonetti, D. Roberto, R. Ugo, A. Valore, L. Falciola, P. Brulatti, M. Cocchi and J. A. G. Williams, *J. Mater. Chem*., 2012, **22**, 10650; (*d*) D. Kourkoulos, C. Karakus, D. Hertel, R. Alle, S. Schmeding, J. Hummel, N. Risch, E. Holder and K. Meerholz, *Dalton Trans*., 2013, **42**, 13612; (*e*) Organic light-emitting diodes: Materials, devices and applications, ed. A. Buckley, Woodhead, Cambridge, 2013, Chapter 3 and 10; (*f*) F. Nisic, A. Colombo, C. Dragonetti, D. Roberto, A. Valore, J. M. Malick, M. Cocchi, G. R. Freemane and J. A. G. Williams, *J. Mater. Chem. C*, 2014, **2**, 1791.
11. A. Poloek, C.-T. Chen and C.-T. Chen, *J. Mater. Chem. C*, 2014, **2**, 1376.
12. S.-H. Liao, J.-R. Shiu, S.-W. Liu, S.-J. Yeh, Y.-H. Chen, C.-T. Chen, T. J. Chow and C.-I. Wu, *J. Am. Chem. Soc.*, 2009, **131**, 763.
13. J. Brooks, Y. Babayan, S. Lamansky, P. I. Djurovich, I. Tsyba, R. Bau and M. E. Thompson, *Inorg. Chem*., 2002, **41**, 3055.
14. Crystal data for **FPtOPhND**: $C_{25}H_{15}F_2N_3O_2Pt$: Fw = 622.49, monoclinoc, $P2_1/c$, Z = 4, $F(000)$ = 1192. Cell dimendions: a = 14.9476(8) Å, b = 19.1171(8) Å, c = 6.8875(3) Å, α = 90°, β = 98.290(4)°, γ = 90°, V = 1947.57(16) Å^3, $2\theta_{max}$ = 50.0°, ρ_{cacld} = 2.123 mg m^{-3}. Of 19303

reflections, 5135 were independence, 298 parameters, R (F_o) = 0.0316 (for reflections with $I > 2\sigma(I)$), R_w (F_o) = 0.0493 (for reflections with $I > 2\sigma(I)$). The GoF on F^2 was equal 1.030. Crystal data for **FPtCzND**: $C_{62}H_{36}F_4N_8O_2Pt_2$: *Fw* = 1390.22, monoclinoc, *C2/c*, Z = 4, *F*(000) = 5376. Cell dimendions: a = 51.3810(14) Å, b = 7.9870(2) Å, c = 26.1603(7) Å, α = 90°, β = 114.761(2)°, γ = 90°, V = 9748.7(5) Å^3, $2\theta_{max}$ = 50.0°, ρ_{cacld} = 1.896 mg m^{-3}. Of 105284 reflections, 9960 were independence, 703 parameters, R (F_o) = 0.0282 (for reflections with $I > 2\sigma(I)$), R_w (F_o) = 0.0707 (for reflections with $I > 2\sigma(I)$). The GoF on F^2 was equal 1.109. CCDC-1010105 and CCDC-1010104 contain the supplementary crystallographic data of **FPtOPhND** and **FPtCzND**, respectively. These data can be obtained free of charge via www.ccd.cam.ac.uk/conts/retrieving.html (or from the Cambridge Crystallographic Data Centre, 12, Union Road, Cambridge CB21EZ, UK; fax: (+44)1223-336-033; or deposit@ccdc.cam.ac.uk).

15. (*a*) L. Chassot, E. Muller and A. V. Zelewsky, *Inorg. Chem*., 1984, **23**, 4249; (*b*) S.-W. Lai, M. C.-W. Chan, T.-C. Cheung, S.-M. Peng and C.-M. Che*, Inorg, Chem*., 1999, **38**, 4046; (*c*) S.-Y. Chang, J.-L. Chen, Y. Chi, Y.M. Cheng, G.-H. Lee, C.-M. Jiang and P.-T. Chou, *Inorg. Chem*., 2007, **46**, 11202.
16. (*a*) B. Yin, F. Niemeyer, J. A. G. Williams, J. Jiang, A. Boucekkine, L. Toupet, H. L. Bozec and V. Guerchais*, Inor. Chem*., 2006, **45**, 8584; (*b*) Z. M. Hudson, C. Sun, M. G. Helander, H. Amarne, Z.-H. Lu and S. Wang, *Adv. Funct. Mater*., 2010, **20**, 3426.
17. (*a*) K. M.-C. Wong and V. W.-W. Yam, Acc. Chem. Res., 2011, **44**, 424; (*b*) E. Rossi, A. Colombo, C. Dragonetti, D. Roberto, F. Demartin, M. Cocchi, P. Brulatti, V. Fattorie and J. A. G. Williams, *Chem. Commun*., 2012, **48**, 3182; (*c*) T. Shigehiro, S. Yagi, T. Maeda, H. Nakazumi, H. Fujiwara and Y. Sakura, *J. Phys. Chem. C*, 2013, **117**, 532; (*d*) P. Brulatti, V. Fattori, S. Muzzioli, S. Stagni, P. P. Mazzeo, D. Braga, L. Maini, S. Militae and M. Cocchi, *J. Mater. Chem. C*, 2013, **1**, 1823; (*e*) L.-M. Huang, G.-M. Tu, Y. Chi, W.-Y. Hung, Y.-C. Song, M.-R. Tseng, P.-T. Chou, G.-H. Lee, K.-T. Wong, S.-H. Cheng and W.-S. Tsai, *J. Mater. Chem. C***,** 2013,**1**, 7582.
18. X.-F. Zhang and W. Guo, *J. Photochem. Photobiol. A: Chem*., 2011, **225**, 117.
19. M. D. Halls and H. B. Schlegel, *Chem. Mater*., 2001, **13**, 2632.
20. G. Schwartz, S. Reineke, T. C. Rosenow, K. Walzer and K. Leo*, Adv. Funct. Mater*., 2009, **19**, 1319.
21. M. S. Lowry, W. R. Hudson, R. A. Pascal, Jr. and S. Bernhard, *J. Am. Chem. Soc*., 2004, **126**, 14129.
22. J. C de Mello, H. F. Wittmann and R. H. Friend, *Adv. Mater.*, 1997, **9**, 230.
23. C.-L. Chiang, M.-F. Wu, D.-C. Dai, Y.-S. Wen, J.-K. Wang and C.-T. Chen, *Adv. Funt. Mater.*, 2005, **15** ,231.
24. M. Thelakkat, H.-W. Schmidt, *Adv. Mater*., 1998, **10**, 219.
25. G.M. Sheldrick, *SHELXL-97*, University of Gottingen, Germany, 1997.
26. L. J. Farrugia, *J. Appl. Cryst*., 1999, **32**, 837.
27. S. R. Forrest, D.D.C. Bradley and M. E. Thompson, *Adv. Mater.*, 2003, **15**, 1043.
28. B. E. Koene, D. E. Loy and M. E. Thompson, *Chem. Mater*., 1998, **10**, 2235.
29. P. J. Low, M. A. J. Paterson, D. S. Yufit, J. A. K. Howard, J. C. Cherryman, D. R. Tackley, R. Brookc and B. Brown, *J. Mater. Chem*., 2005, **15**, 2304.
30. Shi, J.; Tang, C. W.; Chen, C. H. U.S. Patent No. 5645948, 1997.
31. Y. You and S. Y. Park, *J. Am. Chem. Soc*., 2005, **127**, 12438.
32. D. Kourkoulos, C. Karakus, D. Hertel, R. Alle, S. Schmeding, J. Hummel, N. Risch, E. Holder and K. Meerholz, *Dalton Trans*., 2013, **42**, 13612.

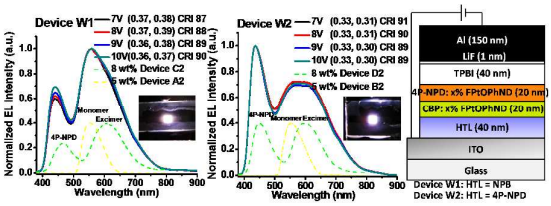

Voltage independent CIE and superb CRI of hybrid white OLEDs based on platinum complex single dopant